Palaeogeography, Palaeoclimatology, Palaeoecology 650 (2024) 112368

Contents lists available at ScienceDirect

Palaeogeography, Palaeoclimatology, Palaeoecology

journal homepage: www.elsevier.com/locate/palaeo

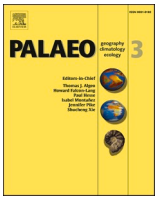

Unlocking the geochemical features of the Paleocene southern Pacific Ocean using carbon isotopes and biolipids

Lian Jiang [a,b,*], Blanca Ausín [c], Sonal Khanolkar [d,e], Yunpeng Wang [a,*], Simon C. George [b]

[a] State Key Laboratory of Organic Geochemistry, Guangzhou Institute of Geochemistry, Chinese Academy of Sciences, China
[b] School of Natural Sciences, Macquarie University, Australia
[c] Geology Department, Salamanca University, Spain
[d] GEOMAR Helmholtz-Zentrum für Ozeanforschung, Kiel, Germany
[e] Department of Earth Sciences, Indian Institute of Technology Gandhinagar, India

ARTICLE INFO

Editor: Prof. M Elliot

Keywords:
International Ocean Discovery Program (IODP)
Expedition 378
Hopanoid
Steroid
New Zealand

ABSTRACT

Little is known about the Paleocene in the southern Pacific Ocean due to scarce marine records. Here, we present a systematic geochemical investigation using biomarkers, carbonate content, and carbon isotopes of a set of early Paleocene deep-sea cores from International Ocean Discovery Program Expedition 378 Site U1553. The results provide a new Paleocene biomarker profile for the Campbell Plateau, New Zealand. The occurrence and distribution of a series of hopenes, ββ hopanes, sterenes and biomarker-based maturity parameters indicate that these organically-lean sediments are in an early diagenetic stage, with an equivalent vitrinite reflectance of approximately 0.4%. Biomarker data (e.g., gammacerane index and homohopane index), carbonate carbon isotopes (−27.9 ‰ to +2.0 ‰) combined with onboard data (sulphur and methane contents) indicate that the redox properties of the Paleocene southern Pacific Ocean changed from an oxidising-anoxic transition zone to a more reducing marine environment (water depth > 1000 m). The sources of the organic matter are diverse, including algae, bacteria, diatoms, dinoflagellates, and higher plants, but are dominated by aquatic organisms. Our new biomarker record bridges a Paleocene biosphere knowledge gap in the high latitude South Pacific.

1. Introduction

As the globe stands on the threshold of major future climate warming, it becomes more urgent to understand how warm-Earth climate systems begin, maintain themselves, and end. The early Paleogene world was a time of extremely warm climates, with fauna and flora in SE Australia and New Zealand typical of modern tropical-subtropical latitudes, and thus is thought to be a good analogue for a future warm-Earth climate system (Gillespie and Burns, 2006). Deep-sea sedimentary records are particularly important because they contain abundant palaeoceanographic and palaeoclimatic information, providing a way of looking back in geological time (Hesse and Schacht, 2011). The Pacific Ocean plays a vital role in the global ecosystem, as it covers nearly one third of Earth's surface. Changes in ocean currents, increases in sea surface temperature, and ocean acidification are closely linked to climate change (Garcia-Soto et al., 2021). Because of restrictions associated with current technical and instrumental limitations, appropriate high-latitude deep-sea cores are unobtainable in the North Pacific, so all known Pacific Ocean records of deep-sea cores are from the South Pacific (Thomas et al., 2020; Röhl et al., 2022).

Currently existing data about the Paleogene in the Pacific Ocean from about 40°S–60°S is from the Deep Sea Drilling Project (DSDP) Legs 29, 35, and 92, and Ocean Drilling Program (ODP) Legs 177, 181, 183, and 189 (Kennett et al., 1975; Leinen et al., 1986; Gersonde et al., 1999; Carter et al., 1999; Coffin et al., 2000; Exon et al., 2004). Most of these old ODP/DSDP sites were drilled from 1973 to 1999, and had low recovery of Eocene sediments, and/or were missing Paleocene sediments. Throughout the South Pacific, the most well-known was DSDP Leg 29 (Site 277), which was drilled on the Campbell Plateau in southern New Zealand and recovered late Paleocene to late Oligocene carbonates, but had relatively low core recovery with only spot-coring (Kennett et al., 1975; Hollis et al., 2014, 2015; Thomas et al., 2020). Thus, International Ocean Discovery Program (IODP) Expedition 378 was designed and drilled in 2020 to resolve these data gaps. Compared to DSDP Site 277, Expedition 378 (Site U1553) has provided a crucial, continuous record of the shallow subantarctic South Pacific from the Paleocene to late

* Corresponding authors at: State Key Laboratory of Organic Geochemistry, Guangzhou Institute of Geochemistry, Chinese Academy of Sciences, China.
E-mail addresses: lian.jiang@mq.edu.au (L. Jiang), wangyp@gig.ac.cn (Y. Wang).

https://doi.org/10.1016/j.palaeo.2024.112368
Received 11 February 2024; Received in revised form 31 May 2024; Accepted 6 July 2024
Available online 10 July 2024

Oligocene (Fig. 1). The expedition acquired 912 m of core from multiple holes through the Paleogene sedimentary section from the southern Campbell Plateau, south of the South Island of New Zealand. Currently, there is no published biomarker data from IODP Expedition 378 (Röhl et al., 2022). Most reports from previous drilled DSDP Site 277 have focused on the Paleocene-Eocene Thermal Maximum and Early Eocene Climatic Optimum-associated events (Hollis et al., 2009, 2014, 2015). The early Paleocene in the southern Pacific Ocean world is unknown to geoscientists, and in particular nothing is known about its biomarkers. This study aims to investigate the organic geochemical characteristics of a series of early Paleocene marine core sediments from this location, build the first early Paleocene biomarker profile, and assess the palaeoclimate conditions and biological productivity, thus enhancing our understanding of the early Paleocene in the South Pacific Ocean.

2. Geological background

The Campbell Plateau is a large submarine plateau with an area of about 800,000 km^2, located in subantarctic New Zealand (Fig. 1), approximately between latitudes 47–55°S (Davey and Houtz, 1977; Cathie, 2020). The geological history of the Campbell Plateau dates back to 98 Ma, when the Zealandia continent originally separated from Gondwana (Cook et al., 1999; King, 2000). The southern margin of the Campbell Plateau was located next to the continental shelves of the eastern Ross Sea and the West Antarctic region of Marie Byrd Land. After the breakup of Marie Byrd Land at approximately 83–79 Ma, the focus of tectonic activity shifted to other areas of the southwestern sector of the Southern Ocean from 80 to 53 Ma, being dominated by seafloor spreading of the Tasman Sea and South Pacific Ocean (Cook et al., 1999). The Campbell Plateau in the Late Cretaceous, however, is interpreted to have been above sea level (King, 2000), and was linked to the evolution of the Great South Basin through the Late Cretaceous to the Paleocene (Grobys et al., 2009; Omosanya and Harishidayat, 2019). In the late Cretaceous, a regional marine transgression occurred across Zealandia, in eastern New Zealand at ~80 Ma and in the west at ~67–65 Ma. During the Eocene, tectonic activity continued on the Campbell Plateau, and seafloor spreading occurred during this period. This spreading continued through the Oligocene to Miocene, and finally resulted in the Campbell Plateau at its current day position (Cook et al., 1999; Cathie, 2020). IODP Expedition 378 (Site U1553) was located at 1221 m water depth on the western margin of the Campbell Plateau (Fig. 1). The lack of seismic data at this site (Röhl et al., 2022) means that more details about the tectonic history and structure of the study area are unknown.

3. Materials and methods

3.1. Samples

The 14 marine sediment cores presented here were collected from Hole U1553D (52°13.4403S', 166°11.4796E'). Basic information about these samples is shown in Table 1. According to the onboard reports (Thomas et al., 2020; Röhl et al., 2022), samples S180, S173, S167, S160, and S151 are from lithological unit Vb, whilst samples S143, S137, S135, S133, S132, S131, S130, and S127 are from lithological unit Va. These are comprised of brown to dark mudstones and dolomitic mudstones, based on observation of hand specimens (Fig. S1 in Appendix) and other onboard analyses (Röhl et al., 2022). Only one sample (Sample S124) is from unit IV, and is a pale dolomitic mudstone (Fig. S1; Table 1).

3.2. Analytical methods

3.2.1. Sample preparation

A half centimetre was removed from the sediment cores using a rock saw (VJ Faceting Machines Childers QLD, 3-in. trim saw), and the inside portion of the samples was rinsed with tap water and then MilliQ water. The wet sediment samples were allowed to dry naturally in a fume cupboard (> 48 h), loosely covered by foil. Dry cores were crushed using a rock mill to <200 mesh, and the powders were stored in glass bottles.

3.2.2. Carbonate content measurement

About 0.05 g of powdered sediment was loaded into a BTX™ III X-ray diffraction (XRD) Analyzer (Olympus). Cobalt was used as the radiation source under the normal voltage of 30 kV and a current of 1/3 mA. The XRD diffraction pattern was recorded for 2θ from 5° to 55°, with 120 exposures for each sample. The total scan time for each sample was approximately 30 min.

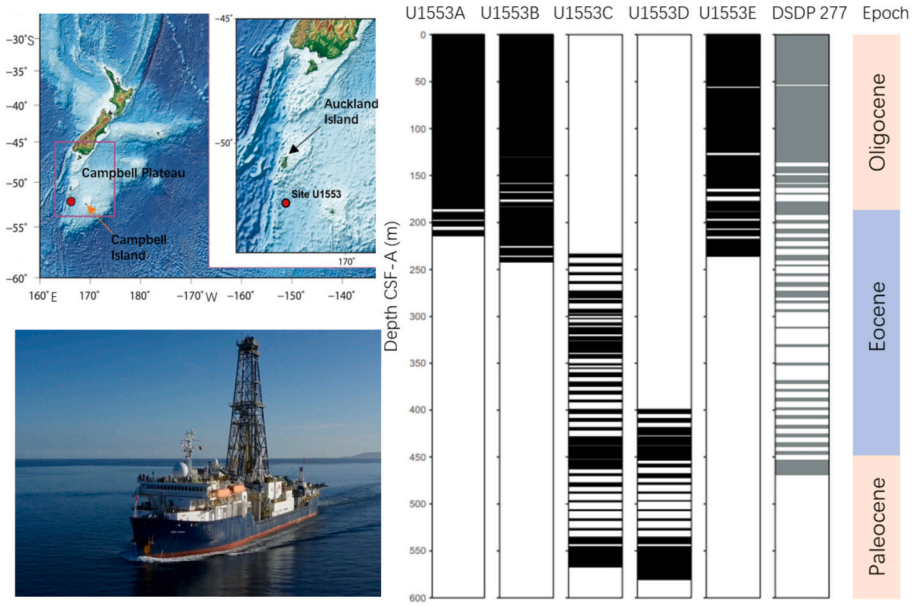

Fig. 1. Top left: Coring location on the Campbell Plateau, offshore New Zealand. Bottom Left: Drill ship JOIDES Resolution on Expedition 378, SW of Lautoka, Fiji (Credit: Phil Christie, Expedition 378). Right: Comparison of Cenozoic core recovery from IODP Expedition 378 (Site U1553) and DSDP Leg 29 (Site 277).

Table 1
Basic information on the early Paleocene samples from U1553D, Campbell Plateau.

Sample code	Core ID	Top offset (cm)	Bottom offset (cm)	Top depth CSF-A (m)	Bottom depth CSF-A (m)	Lithologic unit and description $		$CaCO_3$ (%)	$\delta^{13}C_{carbonate}$ (‰)	Pr/Ph	Pr/*n*-C_{17}	Ph/*n*-C_{18}	CPI_{22-32}	OEP	TAR
S124	9R1W	17	21	467.67	467.70	IV	Limestone. Common to abundant micrite and nannofossils. Variable bioturbation. Quartz and clay increase downwards.	23.8	+2.0	0.67	0.21	0.32	1.05	1.03	31.6
S127	10R1W	42	45	477.64	477.67	Va	Mudstone to	7.8	+1.55	0.81	0.25	0.35	1.04	1.02	17.7
S130	11R1W	74	77	487.74	487.77		dolomitic	8.0	+1.16	1.02	0.25	0.30	1.06	1.04	14.0
S131	12R1W	35	38	497.01	497.04		mudstone,	8.3	+1.48	nd	nd	nd	nd	nd	nd
S132	13R1W	48	52	506.86	506.89		occasionally sandy.	6.7	−0.40	0.62	0.13	0.32	1.05	1.03	32.1
S133	14R1W	18	21	516.26	516.29		Pale yellow-brown	8.0	−2.40	0.92	0.20	0.26	1.05	1.03	22.9
S135	15R1W	40	44	526.34	526.37		coloured matrix	6.6	−1.08	0.87	0.31	0.43	1.06	1.03	11.3
S137	16R1W	70	73	536.30	536.33		composed of clays,	7.1	+0.71	1.04	0.26	0.29	1.03	1.01	25.5
S143	17R2W	63	67	547.43	547.46		calcitic micrite and organic matter. Foraminifers are common and concentrated in mm-scale beds.	6.4	−0.31	1.19	0.56	0.66	1.03	1.01	11.8
S151	18R2W	127	130	557.67	557.70	Vb	Mudstone to	4.4	−27.9	1.26	0.65	0.72	1.02	0.99	7.1
S160	18R7W	47	52	564.76	564.79		dolomitic	5.3	−22.1	1.14	0.73	0.62	1.04	1.03	9.3
S167	19R4W	124	127	570.55	570.58		mudstone,	4.1	−4.12	1.24	0.81	0.69	1.04	1.02	11.4
S173	20R1W	96	100	575.55	575.58		occasionally sandy.	5.6	−1.42	1.74	1.52	1.11	1.04	1.02	9.4
S180	20R5W	34	42	580.91	580.94		Increased bioturbation and sometimes high abundance of secondary dolomite crystals.	4.2	−1.93	1.47	1.05	0.87	1.04	1.01	29.5

Pr = pristane; Ph = phytane; CPI_{22-32} = carbon preference index = $2 \times (n\text{-}C_{23} + n\text{-}C_{25} + n\text{-}C_{27} + n\text{-}C_{29} + n\text{-}C_{31})/(n\text{-}C_{24} + 2 \times n\text{-}C_{26} + 2 \times n\text{-}C_{28} + 2 \times n\text{-}C_{30} + n\text{-}C_{32})$;
OEP = odd-over-even predominance = $1/4 \times (n\text{-}C_{25} + 6 \times n\text{-}C_{27} + n\text{-}C_{29})/(n\text{-}C_{26} + n\text{-}C_{28})$;
TAR = terrigenous/aquatic ratio = $(n\text{-}C_{27} + n\text{-}C_{29} + n\text{-}C_{31})/(n\text{-}C_{15} + n\text{-}C_{17} + n\text{-}C_{19})$; nd = not determined; $ denotes data from Thomas et al. (2020).

3.2.3. Carbon isotope measurement

The stable carbon isotope ratio of bulk carbonate was determined using standard analytical procedures. CO_2 from carbonate in the samples was generated by reaction with 100% phosphoric acid at 72 °C in a special test tube (exetainer) over 1 h, in an online extraction system connected to the inlet of a Thermo Fisher Scientific Delta Plus isotope ratio mass spectrometer. The isotopic composition of the samples is defined and reported in the conventional δ-scale in parts per thousand:

$$\delta^{13}C_{sample}\ (‰) = \left[\left(R_{sample} - R_{standard}\right)/\left(R_{standard}\right)\right] \times 1000$$

where R is the abundance ratio of $^{13}C/^{12}C$ in the sediment samples or in the standard. Isotope ratios are reported relative to the Vienna Pee Dee Belemnite (VPDB) standard for carbon isotope measurements on bulk CO_2. For each sample, the $\delta^{13}C$ value reported herein corresponds to the mean value of three replicate measurements (three replicates on a single exetainer per sample). Precision was monitored by daily $\delta^{13}C$ analysis of a powdered calcite standard (NBS-19) and was 0.1‰ (2σ).

3.2.4. Solvent extraction and fractionation

Total lipid extracts were obtained by accelerated solvent extraction (ASE300) of approximately 35–53 g of powdered sediments using a mixture of dichloromethane (DCM):methanol (MeOH) (9:1, v/v). Before placing in the ASE cylinders, the powdered core samples were mixed with pre-extracted and baked (3 h at 450 °C) sand (approximately 1:1), to improve extraction efficiency. The extraction program for the ASE300 was: initial 5 min. preheating, 5 min. heating to 100°C, 5 min. static extraction, 100% flush of the cylinder, then 300 s. purge with nitrogen under a pressure of 1500 psi. Each sample was run with two cycles, with repacking of the sample/sand mixture in the ASE cylinder between cycles. The resultant extractable organic matter (EOM) was treated with activated and cleaned copper metal to remove sulphides. The EOM was then reduced in volume by rotary evaporation and dried to <1 mL under a stream of N_2. Then, the EOM was separated into fractions (aliphatic, aromatic, and polar) using two-stage gravity column separation on a Pasteur pipette (10 cm × 5.7 mm i.d.) plugged with glass wool and packed with 60–200 μm silica gel (approximately 0.6 g; 45 mm column) that was pre-activated at 120 °C and stored in a desiccator before use. Total hydrocarbons were collected by elution with n-hexane/DCM (4:1 v/v, 3 mL), and polar compounds were collected by elution with MeOH/DCM (1:1 v/v, 3 mL). The total hydrocarbon fraction was further separated by the same sort of column into an aliphatic fraction that was collected by elution with *n*-hexane (~2.6 mL), and an aromatic fraction by elution with *n*-hexane/DCM (4:1; 3.5 mL).

3.2.5. Lipid biomarker analysis

Aliphatic fractions were analysed by gas chromatography–mass spectrometry (GC–MS) on an Agilent gas chromatograph (6890 N) coupled to an Agilent mass selective detector (5975B). An Agilent DB-5MS fused silica column (60 m length × 0.25 mm internal diameter × 0.25 μm film thickness) was used. The oven program started with an injection temperature of 40 °C held for 2 min, followed by a rise of 4 °C min^{-1} until the temperature reached 310 °C, at which it was held for 40 min. The electron ionisation source was operated at 70 eV and helium was used as the carrier gas (constant flow of 1.5 mL/min). Aliphatic fractions were analysed both in full scan (50 to 550 Da) and single ion monitoring (SIM) modes.

Hopanoids and steroids in the aliphatic fractions were further analysed by gas chromatography-triple quadrupole mass spectrometry

(GC–MS/MS) using a Shimadzu GCMS-TQ8050R in multiple-reaction monitoring (MRM) mode. The ion source was operated in EI mode at 250 °C, and argon was used as the collision gas with a collision energy of 6 eV. The oven temperature, program, and column type were the same as for GC–MS analysis.

4. Results

4.1. Basic geochemical properties

Based on onboard geochemical analysis, the Paleocene sediments have low total organic carbon (0.07–0.56 wt%) and sulphur contents (0.14–3.0 wt%; Fig. 2) (Thomas et al., 2020). The XRD analyses indicate that all the samples have a low carbonate content (<10%), except for sample S124 which contains 24% (Fig. 2; Table 1). These data are consistent with the onboard carbonate analysis (Thomas et al., 2020). The $\delta^{13}C$ values of bulk carbonate in the sediments varies from −27.9 ‰ to +2.0 ‰ (Fig. 2; Table 1).

4.2. n-Alkane and isoprenoid distributions

Mass chromatograms (*m/z* 57) of the *n*-alkanes and isoprenoids in two representative samples from IODP Hole U1553D are shown in Fig. S2 in Appendix, with relevant parameters in Table 1. Generally, *n*-alkanes range from *n*-C_{12} to *n*-C_{39}, with a bimodal distribution and maxima at *n*-C_{17} and *n*-C_{27} (Fig. S2). The normalised *n*-alkane profiles (Fig. S3 in Appendix) show that all the samples have a similar distribution, with a very slight odd-over-even predominance (OEP). Both OEP and the carbon preference index (CPI) fall in narrow distribution ranges, with averages of 1.02 and 1.04, respectively (Fig. S4 in Appendix, Table 1). The terrigenous/aquatic ratio (TAR), which is defined as (*n*-C_{27} + *n*-C_{29} + *n*-C_{31})/(*n*-C_{15} + *n*-C_{17} + *n*-C_{19}), is variable, and ranges from 7.1 to 32.1 (Fig. S4). The pristane/phytane (Pr/Ph) ratio ranges from 0.62 to 1.74 with an average of 1.08. The Pr/*n*-C_{17} varies from 0.13 to 1.52 (average = 0.53), and the Ph/*n*-C_{18} ratio varies from 0.26 to 1.11 (average = 0.53; Table 1). There is an increase in Pr/Ph, Pr/*n*-C_{17} and Ph/*n*-C_{18} ratios with increasing depth in Hole U1553D (Fig. S4).

4.3. Hopanoid distributions

Two typical *m/z* 191 mass chromatograms from SIM mode on the Agilent GC–MS show that a series of hopanoids is present in the Site U1553 samples (Fig. S5 in Appendix). Considering the low total organic carbon (TOC; <0.6%) of the Paleocene at Site U1553 (Fig. 2), and the detection sensitivity of this GC–MS, all samples were also analysed by GC–MS/MS for hopanoid determination and identification using MRM. The hopanoids in the studied samples are characterised by hopenes, hopanes and methylhopanes (Figs. S5–S8 in Appendix). Hopenes include the neohop-13(18)-ene series (C_{27}, C_{28}, C_{29}, C_{30} and possible C_{31}) and the hop-17(21)-ene series (C_{27}, C_{29}, C_{30} and C_{31}) (Fig. S6). The C_{27} hopene/C_{27} hopane ratio varies from 0.06 to 0.23 (average = 0.15), and the C_{30} hopene/C_{30} αβ hopane ratio varies from 0.08 to 0.36 (average = 0.20; Table S1 in Appendix). Marine sediments from lithological unit Va have a greater proportion of C_{30} hopenes and a lesser proportion of C_{27} hopenes compared to sediments from lithological unit Vb, and there are consistent trends in both these ratios with depth in Hole U1553D (Fig. 3a,b).

Hopanes identified in the samples include C_{27} hopanes (18α(H)-22,29,30-trisnorneohopane [Ts], 17α(H)-22,29,30-trisnorhopane [Tm], and 17β(H)-22,29,30-trisnorhpane [βTm]), 28,30-bisnorhopane (28,30-BNH) and three unknown C_{28} hopanes, C_{29} hopanes (αβ, βα and ββ isomers) and 18α(H)-30-norneohopane [C_{29}Ts], and C_{30}-C_{35} hopanes (αβ, βα and ββ isomers) (Fig. S7). The Ts/(Ts + Tm) ratio is low, ranging from 0.04 to 0.44 (average = 0.14), and decreases with increasing depth

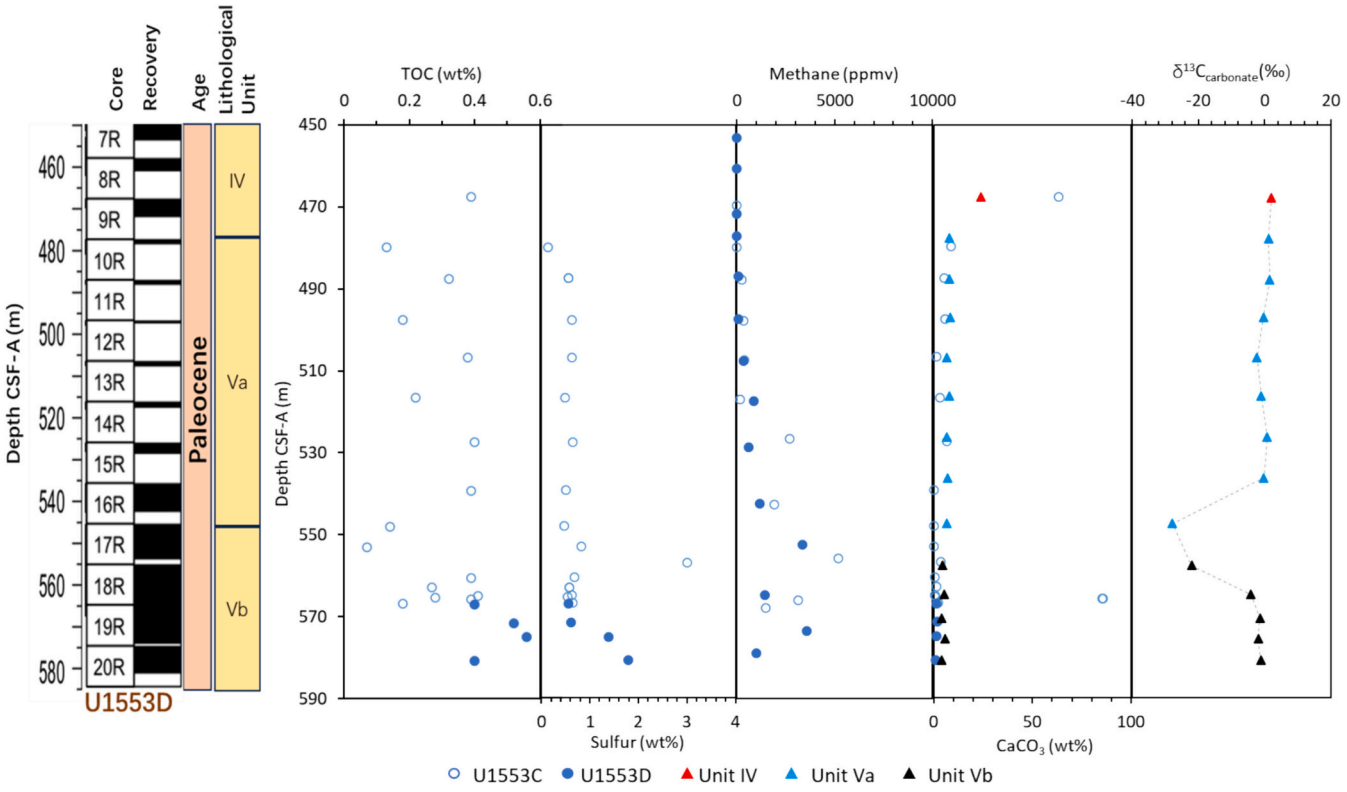

Fig. 2. Depth profile of parameters calculated from onboard data (circles) and this study (triangles) in early Paleocene samples from Site U1553, Campbell Plateau. TOC = total organic carbon. Note that onboard data (TOC, sulphur content, methane concentration, and carbonate content) are from both holes U1553C (open blue circles) and U1553D (filled blue circles) (Thomas et al., 2020). (For interpretation of the references to colour in this figure legend, the reader is referred to the web version of this article.)

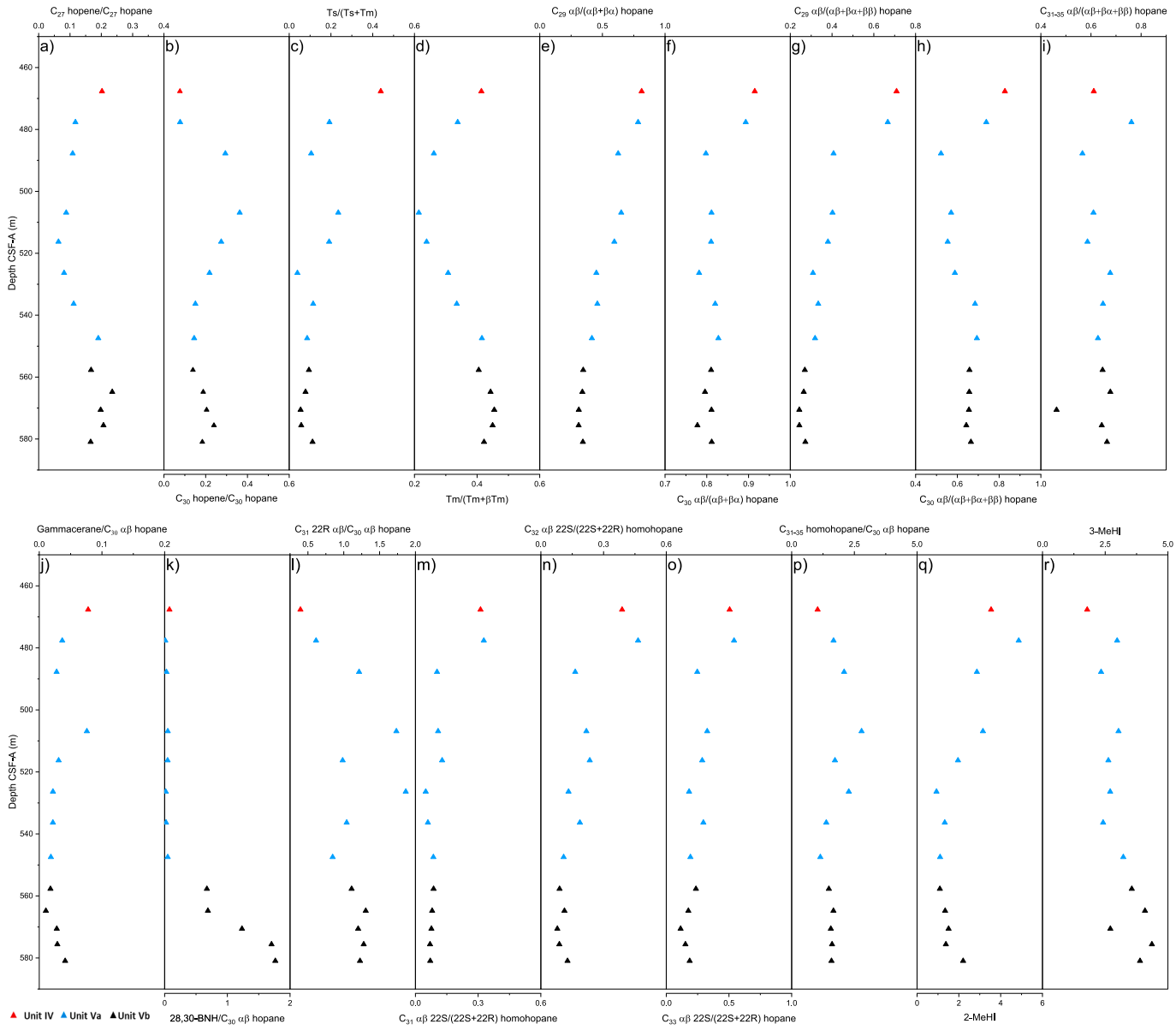

Fig. 3. Depth profile of parameters calculated from hopanoids in early Paleocene samples from Hole U1553D. See Table S1 for definition of abbreviations.

in Hole U1553D (Fig. 3c). The Tm/(Tm + βTm) ratio ranges from 0.21 to 0.45 (average = 0.36) with the lowest values in the middle of lithological unit Va (Fig. 3d). The 28,30-BNH/C_{30} αβ hopane ratio is very variable (0.01–1.77; average = 0.49), with low values (<0.1) in lithological units IV and Va, and a marked increase in lithological unit Vb (Fig. 3k). The C_{29} and C_{30} αβ/(αβ + βα) hopane ratios vary from 0.31 to 0.81 (average = 0.50) and 0.78–0.91 (average = 0.82), respectively (Table S1), and exhibit a slightly decreasing trend with depth in Hole U1553D (Figs. 3e,f). Similarly, the C_{29}, C_{30} and C_{31}-C_{35} αβ/(αβ + βα + ββ) hopane ratios range from 0.24 to 0.71 (average = 0.37), 0.52–0.83 (average = 0.65) and 0.46–0.76 (average = 0.63), respectively, and also decrease with increasing depth in Hole U1553D (Figs. 3g-i). The isomerisation ratio of 22S/(22S + 22R) for the C_{31} homohopanes is relatively low (0.05–0.33; average = 0.12), and is slightly lower in lithological unit Vb (Fig. 3m). The same trend is also observed for the C_{32} 22S/(22S + 22R) homohopanes ratio (0.08–0.46; average = 0.18) and C_{33} 22S/(22S + 22R) homohopanes ratio (0.18–0.54; average = 0.26). The C_{31} αβ hopane (22R)/C_{30} αβ hopane ratio has a wide range of values (0.40–1.87, average = 1.14), with no depth trend (Fig. 3l). The C_{31}-C_{35} homohopanes/C_{30} αβ hopane ratio ranges from 1.03 to 2.79 with an average of 1.6, and has similar values in lithological unit Vb, and more variability in lithological units IV and Va (Fig. 3p). Gammacerane was also identified (Fig. S7) but is in low abundance, with gammacerane/C_{30} αβ hopane ratios varying from 0.01 to 0.08 (average = 0.03; Table S1).

Methylhopanes identified in the samples include C_{30}-C_{33} 2α-methylhopanes (αβ), C_{30}-C_{31} 2β-methylhopanes (αβ), C_{31}-C_{32} 3β-methylhopanes (αβ), C_{32} 2α-methylhopane (βα), and C_{32} 3β-methylhopane (βα) (Fig. S8). Methylhopane indices were calculated for the C_{31} homologs of 2α-methylhopane and 3β-methylhopane, expressed as a percentage value ((C_{31} αβ-methylhopane/(C_{31} αβ-methylhopane + C_{30} αβ-hopane) × 100%). The 2α-methylhopane index (2-MeHI) ranges from 0.9% to 4.9% with an average of 2.1%. The 3β-methylhopane index (3-MeHI) ranges from 1.8 to 4.4% with an average of 3.1%, which is close to the Phanerozoic average of 1–3% (Farrimond et al., 2004). The 2-MeHI slightly decreases with increasing burial depth, whilst 3-MeHI increase with the increasing burial depth in Hole U1553D (Figs. 3q,r).

4.4. Steroid distributions

The distribution of steroids in the samples is complex (Fig. S5), with up to 80 compounds present, including C_{26}, C_{27}, C_{28}, C_{29}, and C_{30} regular steranes, diasteranes, sterenes, diasterenes, methylsteranes and dinosteranes (Figs. S9–S11 in Appendix). Generally, regular steranes predominate over diasteranes in all the samples, with the C_{27} βα diasterane/regular sterane ratio ranging from 0.02 to 0.65 (average = 0.16), and the C_{29} βα diasterane/regular sterane ratio ranging from 0.03 to 0.42 (average = 0.16) (Table S2 in Appendix). C_{26}–C_{30} regular steranes are moderately dominated by C_{27} homologs (C_{27}/C_{29} ααα 20R steranes mostly >1; Fig. 4a,b), while % C_{26} + C_{30} steranes compose <11% of total regular steranes (Fig. 4a). There are three different series of C_{26} steranes in geological samples, namely 24-norcholestanes, 27-norcholestanes and 21-norcholestanes (Holba et al., 1998a, 1998b; Aboglila et al., 2011). Only trace amounts of a 24-norcholestane isomer (?) and 27-norcholestanes are present in the samples, the latter inferred to be dominated by the βαα isomer. The C_{27}–C_{30} regular steranes are also inferred to contain abundant βαα isomers, typical of immature samples, which on the column used co-elute with ααα 20S (C_{27}), αββ 20R (C_{27}–C_{29}), and αββ 20S (C_{30}) isomers. The C_{29} ααα 20S/(20S + 20R) sterane varies from 0.02 to 0.21 (average = 0.09), with no clear depth trend (Table S2). Calculated vitrinite reflectance based on the C_{29} ααα 20S/20R sterane ratio (%VRE; Bein and Sofer, 1987) is 0.34–0.46% (average = 0.38%) (Fig. 5a). The C_{29} αββ/(αββ + ααα) sterane varies from 0.01 to 0.42 with an average of 0.1. The C_{30}/C_{27}-C_{30} ααα 20R sterane ratio is low, varying from 0.02 to 0.08 (average = 0.04) (Table S2; Fig. 4b).

Four types of C_{27}-C_{29} diasterenes occur in the samples, including 10α-diacholest-13(17)-enes, 10β-diacholest-13(17)-enes, 24-methyl-10α-diacholest-13(17)-enes, 24-methyl-10β-diacholest-13(17)-enes, 24-ethyl-10α-diacholest-13(17)-enes, and 24-ethyl-10β-diacholest-13(17)-enes (all with 20S and 20R isomers) (Fig. S10). C_{27}-C_{29} sterenes with three different double bond positions occur in the samples, including cholest-4-ene, cholest-2-ene, cholest-5-ene, 24-methylcholest-4-ene, 24-methylcholest-2-ene, 24-methylcholest-5-ene, 24-ethylcholest-4-ene, 24-ethylcholest-2-ene, and 24-ethylcholest-5-ene (Fig. S10). The C_{27} diasterenes/C_{27} sterenes ratio varies from 0.09 to 0.47 (average = 0.24), and the C_{29} diasterenes/C_{29} sterenes ratio varies from 0.05 to 0.36 (average = 0.21; Table S2), both ratios increasing with depth (Fig. 4b).

Two types of methylsteranes (3β- and 4α-) and dinosteranes are present in the sediments (Fig. S11 in Appendix). The 3β-methylsteranes include 3β-methyl-5α,14α,17α-cholestane 20R, 3β-methyl-5α,14α,17α-methylcholestane 20R, and 3β-methyl-5α,14α,17α-ethylcholestane 20R. The 4α-methylsteranes include 4α-methyl-5α,14α,17α-cholestanes, 4α-methyl-5α,14α,17α-methylcholestanes, and 4α-methyl-5α,14α,17α-ethylcholestanes (all with 20S and 20R isomers), 4α-methyl-5α,14β,17β-cholestane 20S, 4α-methyl-5α,14β,17β-methylcholestane 20S, and 4α-methyl-5α,14β,17β-ethylcholestane 20S. The $C_{30}/(C_{28}$-$C_{30})$ methylsterane ratio varies from 1.2 to 1.9 (average = 1.4), and decreases with increasing depth (Fig. 4b). The dinosterane/C_{30} methylsterane ratio varies from 0.04 to 0.39 (average = 0.14), with slightly higher values in lithological unit Va (Table S2; Fig. 4b).

5. Discussion

5.1. Thermal maturity

The thermal maturity of the Hole U1553 marine sediments can be evaluated by biomarker distributions and related thermal maturation

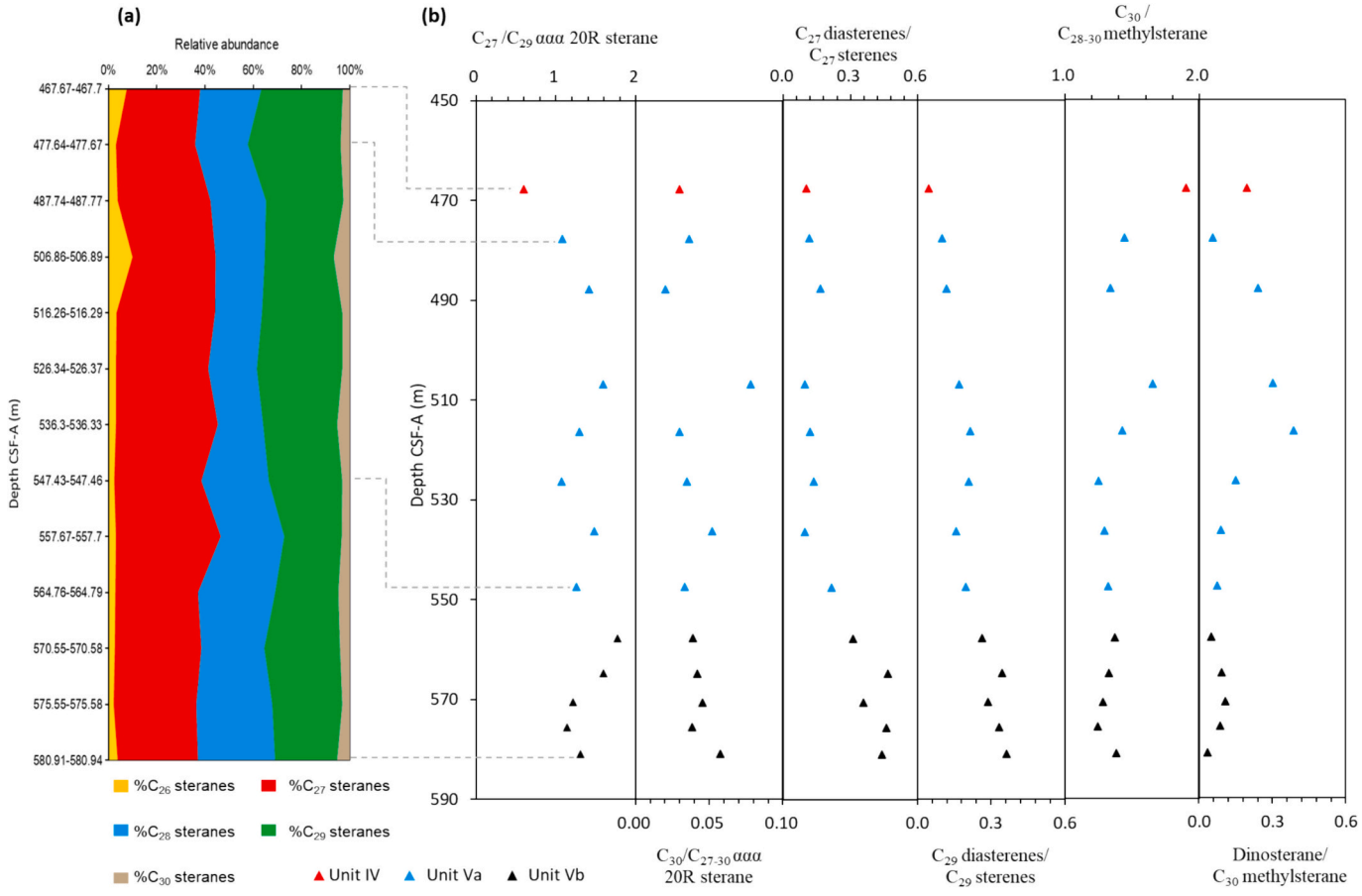

Fig. 4. Steroid parameters with depth in early Paleocene samples from Hole U1553D. a) Diagram showing the relative distribution of $\%C_{26}$-C_{30} regular steranes, and b) Ratios calculated from steroids. See Table S2 for definition of abbreviations.

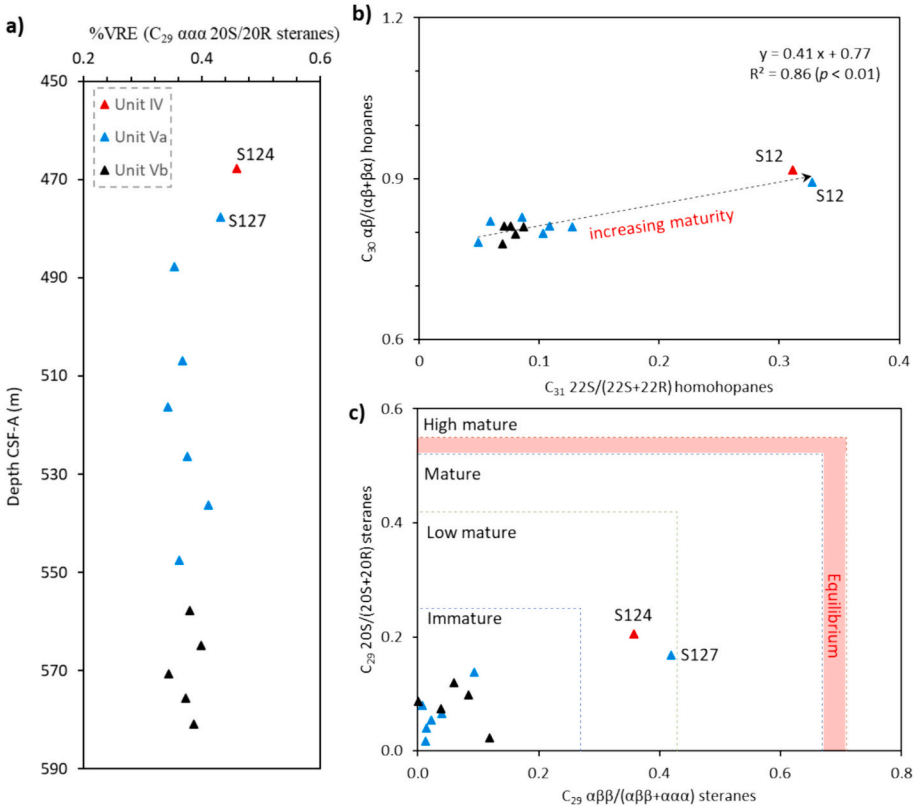

Fig. 5. Thermal maturity parameters in Paleocene samples from U1553D. a) Depth profile of vitrinite reflectance equivalent based on C_{29} ααα 20S/20R steranes (% VRE). b) Cross-plot of C_{31} 22S/(22S + 22R) homohopanes versus C_{30} αβ/(αβ + βα) hopanes. c) Cross-plot of C_{29} ααβ/(ααβ + ααα) steranes versus C_{29} 20S/(20S + 20R) steranes (after Seifert and Moldowan, 1986). See Table S2 for definition of abbreviations. Note that C_{29} αββ sterane (20R) co-elutes with C_{29} βαα sterane (20R) in the metastable transition 400.4 → 217.2 (Fig. S9). Here we assume that the area of C_{29} αββ sterane (20R) peak is the same as the C_{29} αββ sterane (20S) peak in order to calculate the C_{29} αββ/(αββ + ααα) steranes ratio.

parameters. *n*-Alkane distributions are controlled by the organic matter source, but are also influenced by thermal maturity. For instance, *n*-C_{15}, *n*-C_{17} and *n*-C_{19} are thought to originate from aquatic organic matter, while *n*-C_{27}, *n*-C_{29} and *n*-C_{31} are more abundant in land-plant-derived organic matter (Tissot and Welte, 1978), although some non-marine algae (e.g. *Botryococcus braunii*) may contribute to a 'saw-toothed' profile of C_{21}–C_{31} *n*-alkanes and ^{13}C-enriched even *n*-alkanes (Moldowan et al., 1985; Grice et al., 2001; Dawson et al., 2004). The *n*-alkane ratios OEP and CPI can reflect both the thermal maturity and source input of organic matter, both decreasing with increasing thermal maturity. High CPI values indicate low maturity and land-plant input, while CPI values for high-molecular-weight *n*-alkanes close to 1.0 can be due to biodegradation, microbial and algal inputs, or contamination with petroleum (Clark and Blumer, 1967; Volkman et al., 1984; Rieley et al., 1991). The OEP and CPI ratios in all the samples are around 1.0, with a very slight odd-over-even predominance (Table 1; Fig. S4). This might indicate a mature stage for the organic matter, but this is inconsistent with all the other biomarker distributions, including the abundant hopenes and sterenes. These *n*-alkane distributions are interpreted to be due to a predominance of marine algal input to the marine core sediments, and/or microbial input in the sediments after burial.

With increasing thermal maturity, the relative abundance of βTm decreases because it is thermally unstable compared to Ts and Tm, so the occurrence of βTm usually indicates an early diagenetic stage (Hong et al., 1986). βTm occurs in all the samples in greater abundance than Tm (Fig. 3), suggesting a low thermal maturity for the U1553D sediments. Likewise, the widespread occurrence of C_{29}-C_{35} ββ hopanes, C_{27}-C_{31} neohop-13(18)-enes and hop-17(21)-enes, and C_{27}-C_{29} diasterenes and sterenes directly corroborate that these sediments are in an early diagenetic stage (Figs. S6–S8, S10).

The 22S/(22S + 22R) isomerisation ratio for C_{31} homohopanes is often used as a maturity index in petroleum and sediments, and increases from 0 to ~0.6 with increasing thermal maturity, reaching equilibrium values at about 0.57–0.62% vitrinite reflectance equivalent (VRE) (Seifert and Moldowan, 1980; Peters et al., 2005). The low C_{31} 22S/(22S + 22R) homohopane ratios (average = 0.12) show a low thermal maturity for all the samples (Fig. 3m; Table S1), probably about 0.4% VRE based on Peters et al. (2005). Similarly, the low C_{32} 22S/(22S + 22R) homohopane (average = 0.18) and C_{33} 22S/(22S + 22R) homohopane (average = 0.26) ratios suggest an immature thermal stage (Figs. 3n-3o; Table S1). These and other hopane-derived maturation parameters (Ts/(Ts + Tm), C_{29} αβ/(αβ + βα) hopane and C_{30} αβ/(αβ + βα) hopane) slightly decrease with increased depth of burial (Figs. 3e-3f), possibly suggesting a slightly higher thermal maturity for the upper sediments from lithological units IV and Va, compared to the deeper sediments from lithological unit Vb in Hole U1553D. The VRE based on C_{29} ααα 20S/20R steranes (Bein and Sofer, 1987; 0.36–0.48%, average = 0.4%, Table S1) is also consistent with immature organic matter in the Paleocene in Hole U1553D, with a slightly higher thermal maturity in the upper two samples (S124 and S127) (Fig. 5a). The cross-plot of two sterane isomerisation parameters (C_{29} ααβ/(ααβ + ααα) sterane and C_{29} 20S/(20S + 20R) sterane; Seifert and Moldowan, 1986) also indicate most samples are immature, with samples S124 and S127 from the low mature stage (Fig. 5c). The reversed thermal maturity gradient based on hopanoids and steroids is also consistent with the general increase in the Pr/*n*-C_{17} and Ph/*n*-C_{18} ratios with depth in Hole U1553D (Fig. S4), because generally, the formation of *n*-alkanes with increasing thermal stress leads to dilution of earlier generated isoprenoids (Tissot and Welte, 1978). The VRE of 0.4% in lithological unit Vb is equivalent to about 62 °C maximum paleo-temperature, based on a correlation

between vitrinite reflectance and temperature (Barker and Pawlewicz, 1994).

The reason for the slightly lower apparent thermal maturity in lithological unit Vb in Hole U1553D is not immediately clear. There is no evidence for a reversed geothermal gradient, for example caused by an igneous intrusion higher in the stratigraphy, so this is an unlikely explanation. One possibility is that the organic matter in the stratigraphically-higher samples has been over-printed by re-worked organic matter that has a higher thermal maturity. A second possibility is that the steroid and hopanoid thermal maturity parameters have been affected by different diagenetic conditions in lithological unit Vb, which have retarded the normal isomerisation reactions that lead to changes in these maturity parameters. Without further information it is not possible to distinguish between these options.

5.2. Depositional environment

The sedimentary conditions during the deposition of marine sediments from Hole U1553D were ascertained by the relative contents of Pr and Ph, the distribution of C_{31}-C_{35} homohopanes, and the relative abundance of C_{27}-C_{29} regular steranes. In general, high Pr/Ph ratios (>3.0) indicate terrigenous organic matter input deposited under oxidising environments, while low ratios (Pr/Ph <0.8) represent anoxic environments sometimes associated with evaporite and carbonate deposition (Didyk, 1978). The relatively low Pr/Ph ratios (Fig. S4, Table S1) and the position of the samples on the Pr/*n*-C_{17} versus Ph/*n*-C_{18} cross-plot show that the early Paleocene marine sediments were deposited under a redox transitional zone to reducing environment (Fig. 6). The downhole trends of Pr/Ph, Pr/*n*-C_{17} and Ph/*n*-C_{18} increasing with depth in Hole U1553D (Fig. S4) may suggest that redox properties changed from sub-oxidising/sub-anoxic conditions in lithological unit Vb, to relatively reducing in lithological units Va and IV.

28,30-Bisnorhopane originates from chemoautotrophic bacteria that grow at the oxic-anoxic interface, such as *Beggiatoa* (a ~ 200-μm diameter sulphur-oxidising bacterium) (Williams, 1984). These bacteria usually form dense filamentous mats with other related microorganisms at the oxic–anoxic transitional zone in environments supplied with hydrogen sulphide, often in marine sediments associated with hydrothermal vents (Brune et al., 2000). With increasing burial depth there is a marked increase in the abundance of 28,30-bisnorhopane relative to C_{30} αβ hopane (Fig. 3k), which occurs exactly at the transition from lithological units Vb to Va. This is anticipated to be due to greater sulphur supply in the deeper sediments (> 560 CSF-A m; Fig. 2) that may have resulted in blooms of the precursors of 28,30-bisnorhopane at the redox interface (1.0 < Pr/Ph < 2.0). However, there is no evidence for water-column stratification (Sinninghe Damsté et al., 1995), as the gammacerane/C_{30} αβ hopane ratio is <0.1 (Table S1; Fig. 3j). High 2-MeHI values (9–32%) generally correspond to low-palaeolatitude, evaporitic and carbonate-rich sediments in the Phanerozoic (Summons et al., 1999), whilst most Cenozoic sediments in high-palaeolatitudes have lower 2-MeHI (<5%) (Knoll et al., 2007). Consistently high 2-MeHI values (9–11%) appear to correlate with dolomite abundance for samples in shallow-water settings, while lower and more variable 2-MeHI values (4–11%) are typical of relatively deeper water environments (i.e., slope to basin) in the Neoarchean (Eigenbrode et al., 2008). The low 2-MeHI (0.9–4.9%) values in Hole U1553D are thus consistent with a high-paleolatitude setting and a deep-water environment (discussed below).

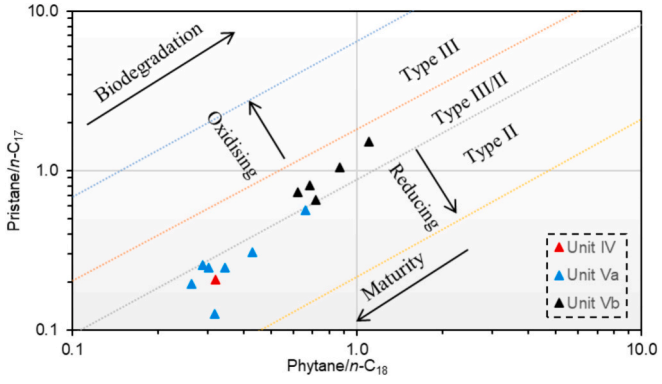

Fig. 6. Cross-plot of phytane/*n*-C_{18} and pristane/*n*-C_{17} for the Paleocene samples from Hole U1553D (after Shanmugam, 1985).

In comparison to lacustrine-derived oils, oils sourced from marine shales, carbonates, and marls usually have a C_{31} αβ hopane (22R)/C_{30} αβ hopane ratio > 0.25 (Peters et al., 2005). The high C_{31} αβ hopane (22R)/C_{30} αβ hopane ratios for the studied samples (0.4–1.9) are therefore consistent with a marine depositional environment. The distribution of C_{31}-C_{35} homohopanes can indicate the redox properties under which marine sediments were deposited (Peters et al., 2005). High values of the homohopane index, which can be expressed as a percentage of C_{35}/(C_{31}-C_{35}) homohopanes (Table S1), indicates anoxic conditions, although this parameter is also influenced by thermal maturity and biodegradation (Peters and Moldowan, 1991). Considering that all the sediments are immature, the homohopane distribution pattern and the homohopane index are inferred to be good redox indicators in Hole U1553D. There is variability in the distribution of C_{31}-C_{35} homohopanes, with some samples having elevated C_{35} homohopanes compared with C_{34} homohopanes (Fig. S12a). The homohopane index has a negative relationship with increasing burial depth, indicating generally more reducing conditions during deposition of lithological unit Va in comparison to lithological unit Vb (Fig. S12b). Similarly, on the C_{27}/C_{29} ααα sterane versus Pr/Ph cross-plot, samples from lithological unit Vb fall in the suboxic-anoxic zone, while samples from lithological unit Va are located in the suboxic-anoxic to anoxic zones (Fig. 7a). These results corroborate the interpretation of the Pr/Ph ratio.

Onboard microfossil observation has shown that radiolarian occurrence in the Paleocene is sporadic, and preservation is poor (Röhl et al., 2022). Barren to rare calcareous nannofossils and planktic foraminifera are found in sediments below ~480 m CSF-A in Hole U1553D (Röhl et al., 2022). Benthic foraminifera are absent in sediments below 510 m CSF-A, but are "few to common" in sediments between 440 and 510 m CSF-A in Hole U1553D. In the Paleocene, a mid-lower bathyal palaeodepth (~1000–1200 m) is inferred by the occurrence of the benthic foraminifers *Bathysiphon* spp., *Gavelinella beccariiformis*, and *Nuttallides truempyi* (Tjalsma and Lohmann, 1983; Hornibrook et al., 1989; Alegret and Thomas, 2013; Röhl et al., 2022). Redeposition of Paleocene or older sediments is suggested by the frequent presence of large, broken specimens of the genus *Lenticulina* and bryozoan fragments, which are inferred to have been derived from shelf environments (e.g., in sediments about 467–497 m CSF-A in Hole U1553D). Additionally, the isobath of DSDP 277 was inferred to be between 1500 and 2000 m (Davey and Houtz, 1977). This is also consistent with a deep-water environment hypothesis indicated by 2-MeHI.

In summary, sediments from Hole U1553D were deposited in a suboxidising to anoxic marine shelf environment. The environment changed from an oxic-anoxic transition zone with strong sulphur supply during deposition of lithological unit Vb, to more reducing conditions during deposition of lithological unit Va.

5.3. Origins of organic matter

The *n*-alkane distributions in the U1553D Paleocene samples are bimodal with maxima at *n*-C_{17} and *n*-C_{27} (Figs. S2–S3), showing a mixed organic matter origin from both aquatic and terrigenous inputs. This result is also confirmed by the cross plot of Ph/*n*-C_{18} and Pr/*n*-C_{17} (Fig. 6), which indicates that the dominant kerogen types are Type II/III and Type III. The TAR is commonly used to quantify the contribution of terrigenous and aquatic organic matter to sediments (Peters et al.,

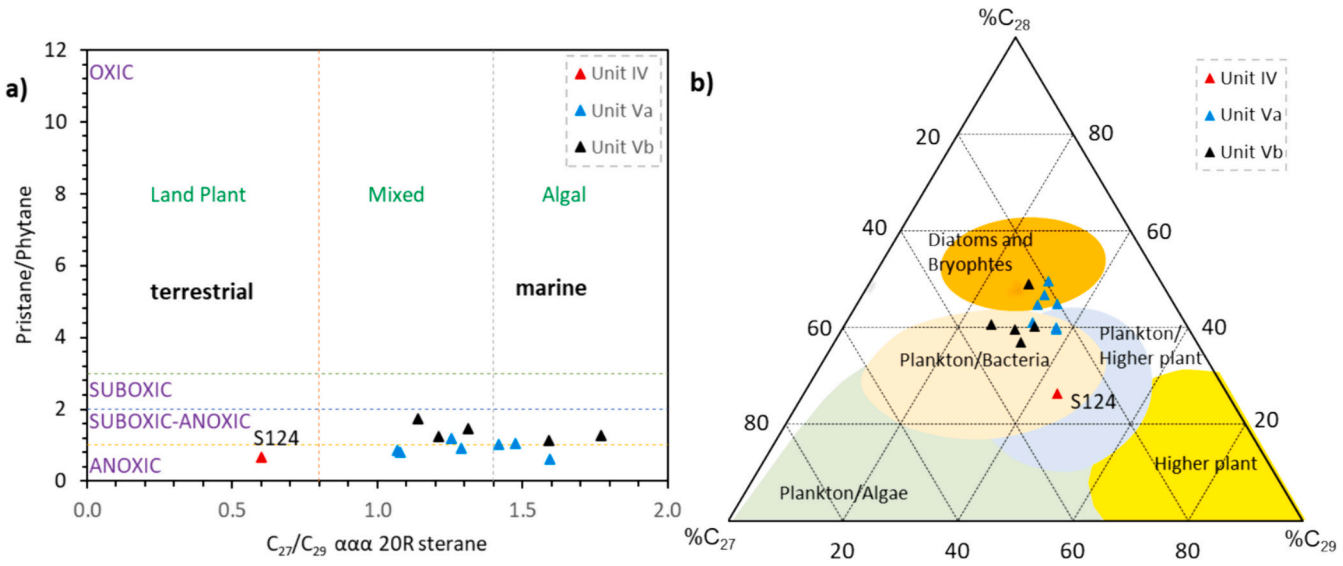

Fig. 7. Biomarker source parameters for the Paleocene samples from Hole U1553D. a) Cross-plot of the C_{27}/C_{29} ααα 20R sterane ratio versus the pristane/phytane ratio (fields are after Gorter, 2001). b) Ternary diagram of $\%C_{27}$, $\%C_{28}$, $\%C_{29}$ ααα 20R steranes (fields are after Moldowan et al., 1985).

2005). The fluctuation of the TAR through the Paleocene in Hole U1553D may reflect variable contributions of aquatic organisms and higher plants to the organic matter over time (Fig. S4 in Appendix).

Hopanoids in geological samples are derived from bacteria (Ourisson et al., 1987). Specifically, C_{27}-C_{35} hopanes arise from the degradation of C_{35} bacteriohopanepolyols (BHPs), which are synthesised by nonspecific bacteria (Rohmer et al., 1984). 2-Methyl-BHPs are functionalised precursors of 2-methylhopanes and mainly produced by taxonomically diverse cyanobacteria, and thus were proposed as molecular proxies for oxygenic photosynthetic cyanobacteria (Summons et al., 1999). However, an anoxygenic phototroph, *Rhodopseudomonas palustris* TIE-1, can produce 2-methyl-BHPs when grown under strictly anaerobic conditions (Rashby et al., 2007). Alphaproteobacteria are now known to also produce 2-methyl-BHPs (e.g., Welander et al., 2010; Ricci et al., 2014), although recent work has suggested that 2-methylhopanes are reliable biomarkers for cyanobacteria prior to 750 Ma (Hoshino et al., 2023). The presence of abundant 2α-methylhopanes in the Paleocene in U1553D (Fig. S8 in Appendix) could be due to either cyanobacteria and/or alphaproteobacteria, and this contribution was more important in the upper part of lithological unit Va and in lithological unit IV (Fig. 3q). 3β-Methylhopanes were also detected, and likely originate from 3-methyl-BHPs that are known to be produced by aerobic respiring methanotrophic and acetic acid bacteria (Rohmer et al., 1984; Zundel and Rohmer, 1985). The generally increasing 3-MeHI with depth in Hole U1553D may record blooms of methanotrophs, consistent with high concentrations of methane in the lower part of lithological unit Vb (Fig. 2). Overall, a diverse range of bacteria contributed to the organic matter in the Paleocene in U1553D.

Steranes in sediments mainly come from sterols, which are important components of the membranes of all eukaryotic organisms (Volkman, 2003). C_{27} regular steranes are indicative of marine zooplankton and algal sources, while C_{29} regular steranes are usually considered to originate from higher plants, although can be derived from marine phytoplankton (Volkman, 1986). A high abundance of C_{28} regular steranes is typically indicative of a contribution from phytoplankton and algae (Huang and Meinschein, 1979; Volkman, 2005). Additionally, the relative abundance of C_{28} steranes varies over geological time, with a significantly higher proportion of C_{28} steranes (C_{28}/C_{29} sterane >0.6) in the Jurassic and Cretaceous, which may be related to the increased diversification of phytoplanktonic assemblages (i.e., diatoms, coccolithophores, and dinoflagellates) (Grantham and Wakefield, 1988). The C_{26} 27-norcholestanes and 24-norcholestanes have been reported in crude oils and sediments (Holba et al., 1998a; Holba et al., 1998b; Rampen et al., 2007), and are attributed to diatoms (Volkman, 2003). C_{30} 24-*n*-propylcholestanes are common in marine environments and are thought to be derived from photosynthetic chrysophyte algae (Moldowan et al., 1990).

Small amounts of 27-norcholestane and possibly a peak due to a 24-norcholestane isomer occur in the Paleocene in Hole U1553D, indicating a diatom contribution to organic matter (Fig. 4). The relative abundance of C_{27}-C_{29} regular steranes is widely used to assess the origin of organic matter in sediments (Moldowan et al., 1985). The ternary diagram of $\%C_{27}$-C_{28}-C_{29} ααα 20R steranes indicates a mixed input of organic matter from plankton, bacteria, diatoms and higher plants for most of the samples, but a predominance of higher plant input to the organic matter in the sample from lithological unit IV (Fig. 7b). There is some clustering of the samples from lithological units Va and Vb, indicating a subtle change in organic matter input between these lithological units. This result is consistent with the analysis based on the cross-plot of C_{27}/C_{29} ααα 20R sterane and Pr/Ph (Fig. 7a). The occurrence of 24-*n*-propylcholestanes reflects a marine algal contribution to the organic matter during deposition. Slightly higher $C_{30}/(C_{27}$-$C_{30})$ ααα sterane and C_{27}/C_{29} 20R ααα sterane ratios with increasing burial depth (Fig. 4b) indicate more abundant aquatic organisms contributing to the organic matter in lithological unit Vb.

Dinosteranes have been detected in dinoflagellate cyst-rich Jurassic marine sediments (Goodwin et al., 1988) and Paleogene terrigenous deposits (Ji et al., 2011). Dinosteranes are thus mainly regarded as indicators for dinoflagellates, although a diatom species has been reported to contain similar sterols (Volkman et al., 1993). The distribution of dinoflagellate cysts depends upon paleoenvironmental conditions, such as coastal/oceanic settings that are highly enriched with nutrients and characterised by a stratified water column (Moldowan and Talyzina, 1998; Palliani and Riding, 2003). Kenig et al. (1995) suggested that dinosteranes and their derivatives in geological samples has been linked to euphotic zone anoxia during deposition of organic matter from algal primary producers. In addition, dinoflagellates are probably the main source of aromatic steroids bearing a methyl group at the C-4 position, for instance 4α-methylcholestane, 4α-methyl-24-methylcholestane and 4α-methyl-24-ethylcholestane (Aboglila et al., 2011). The presence and abundance of dinosteranes and 4α-methyl-24-ethylcholestanes in the Paleocene in Hole U1553D can thus be considered as evidence for dinoflagellates existing in the paleowater column during the early Paleocene in the south Pacific. A greater portion of dinoflagellates

contributing to the organic matter is indicated by the higher dinosterane/C_{30} methylsterane ratios in lithological unit Va in comparison to lithological unit Vb (Fig. 4g).

In summary, the distribution of hopanes, methylhopanes, %C_{26}-C_{30} regular steranes, C_{27}-C_{29} methylsteranes, dinosteranes, and parameters based on these compounds (Figs. S5–S12) reflect the variable planktonic (e.g., diatoms and dinoflagellates), bacterial (e.g., cyanobacteria and/or alphaproteobacterial, and methanotrophic bacteria), algal (e.g., chrysophyte algae), and higher plant contributions to the organic matter in the early Paleocene in the southern Pacific Ocean.

5.4. Depositional model for lithological units Va and Vb

Based on a tectonic reconstruction (Cande and Stock, 2004), IDOP Expedition 378 Site U1553 was located in a relatively restricted marine setting during the early Paleocene (~65 Ma) (Fig. 8a). On the basis of the data from lipid compositions and carbonate isotopes, a depositional model for the early Paleocene at this site is conceived (Fig. 8b).

A sudden increase in methane concentrations in both holes at U1553 occurred at ~488 m CSF-A, coincident with a strong hydrocarbon gas smell and a drastic change from white to grey core material that corresponds to the transition from lithostratigraphic unit IV to unit V based on onboard observations (Fig. 2; Röhl et al., 2022). The methane increase was accompanied by the onboard detection of thermogenic hydrocarbons (C_2, C_3, and C_4) beginning at 542 m CSF-A, suggesting in situ methane production, possibly by microbial activity, and thermogenic gas upward migration (Thomas et al., 2020; Röhl et al., 2022). The carbonate isotope excursion to more negative values occurs between 547 and 557 m CSF-A, and corresponds to the depth interval in which the highest methane and sulphur concentrations were detected (~552–556 m CSF-A; Fig. 2). It also co-occurs with the lithological change from lithological unit Vb to Va, in which less bioturbation and secondary dolomite crystals are present. The negative $\delta^{13}C$ values of bulk carbonate probably result from carbon dioxide produced by bacterial or inorganic oxidation of methane (Freeman et al., 1990). There are also high methane concentrations deeper in unit Vb, without any corresponding carbonate isotope excursion, suggesting that incorporation of isotopically light carbon from the methane into the carbonate was focussed at the unit boundary due to the subtle change in lithology acting as a biogeochemical barrier. Common and diverse trace fossils and bioturbation was observed in many of the cores from lithological units Va and Vb, suggesting an active ecosystem thriving with a variety of organisms. The change in depositional environment from lithological unit Vb to unit Va, and the lesser supply of sulphur and the lower concentration of methane with decreasing depth in Hole U1553 (Fig. 2) are associated with relatively lower 28,30-BNH/C_{30} αβ hopane ratios and 3-MeHIs in lithological unit Va (Figs. 3k,r). These observations are consistent with a methanotrophic-driven system in lithological unit Vb. The moderate Pr/Ph, Pr/*n*-C_{17} and Ph/*n*-C_{18} ratios (Table 1), the relatively high 28,30-BNH/C_{30} αβ hopane ratio (Fig. 3k) and the low homohopane index (Fig. S12b in Appendix) indicate that the depositional environment of lithological unit Vb was in the oxic-anoxic transition zone (Fig. 8b2). A sea level rise led to the focus of deposition in lithological unit Va at Site U1553 to be in deeper water. This is consistent with the biomarker data for lithological unit Va, which show lower Pr/Ph, Pr/*n*-C_{17} and Ph/*n*-C_{18} ratios (Table 1), a lower 28,30-BNH/C_{30} αβ hopane ratio (Fig. 3k), and a relatively high homohopane index (Fig. S12a), which together suggest a more reducing environment

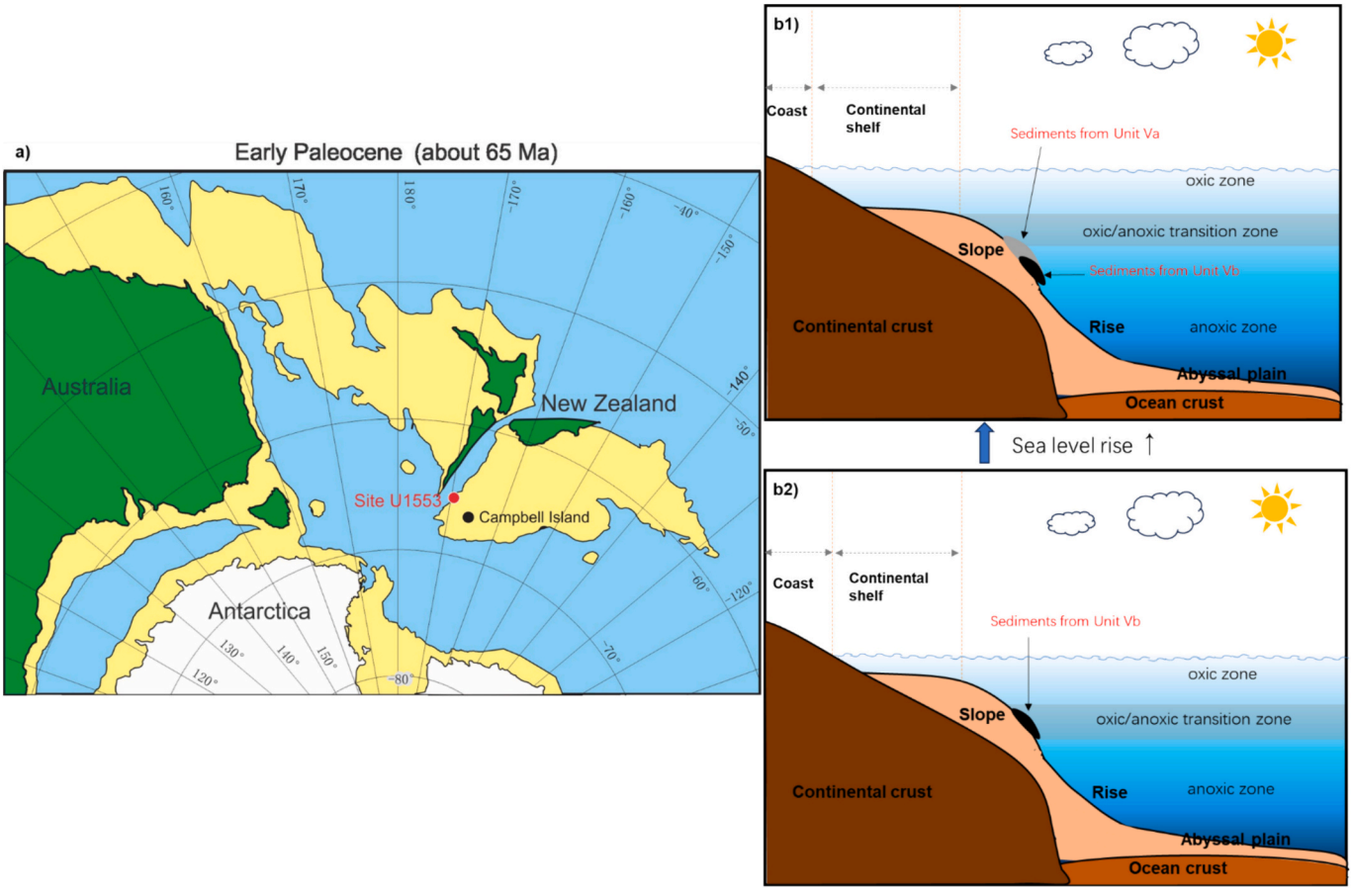

Fig. 8. a) Location of IODP 378 Site U1553 on a tectonic reconstruction for the southwest Pacific during the early Paleocene (~65 Ma) (modified from Cande and Stock, 2004). b1-b2) Depositional models describing the lithological unit Va and Vb deposits in Hole U1553D.

(Fig. 8b1). This hypothesis is also supported by 2-MeHI, the abundance of dinosteranes, and the $\%C_{26}$ regular steranes (Figs. 3–4; Table S2), which here we infer were associated with oxygenic photosynthetic cyanobacteria, dinoflagellates, and diatoms, respectively. In the southern Pacific palaeo-ocean, phytoplankton (including diatoms) and oxygenic photosynthetic cyanobacteria used sunlight as primary producers in the photic zone (<200 m). Zooplankton (including dinoflagellates), which fed on the phytoplankton, were also active in the photic zone. When these organisms died, they underwent decomposition and then settled to the deep, aphotic ocean floor, where they were buried. The redox conditions during the burial process of the sediments therefore directly influenced the preservation of organic matter. During deposition of lithological unit Vb, phytoplankton and zooplankton were buried in an oxic-anoxic transition zone, with relatively low values of 2-MeHI, dinosterane/C_{30} methylsterane ratio, and $\%C_{26}$ regular steranes (Tables S1-S2). Sea level rose from deposition of lithological unit Vb to lithological unit Va. This is inferred to have led to greater phytoplankton and zooplankton productivity in the photic zone, and when these were buried in deeper water there were better preservation conditions (a more reducing environment), leading to relatively higher values of 2-MeHI, dinosterane/C_{30} methylsterane, and $\%C_{26}$ regular steranes in lithological unit Va (Figs. 3–4; Tables S1-S2).

6. Conclusions

We have presented a new comprehensive biomarker profile for the early Paleocene from IODP expedition 378, Site U1553 on the Campbell Plateau, New Zealand. Our results show that the Paleocene sediments were deposited in a sub-oxidising to reducing marine environment on the continental slope, with water depths >1000 m. These sediments are at an immature stage, corresponding to a vitrinite reflectance equivalent of approximately 0.4%, or about 62 °C maximum palaeo-temperature. There is evidence for slightly higher apparent thermal maturity in the younger lithological unit Va, which could be due to over-printing by reworked and more mature organic matter, or different diagenetic conditions in lithological unit Vb which retarded the normal biomarker isomerisation reactions. The origin of the organic matter was a mixture of aquatic organisms (algae, bacteria, plankton, dinoflagellates, and diatoms) and higher plants, but was dominated by aquatic organisms. These results help resolve the biomarker gap for the high latitudes in the South Pacific, and contribute to deepening our understanding of the deep sea biosphere across the Paleocene.

CRediT authorship contribution statement

Lian Jiang: Writing – review & editing, Writing – original draft, Visualization, Validation, Methodology, Investigation, Funding acquisition, Formal analysis, Data curation, Conceptualization. **Blanca Ausín:** Writing – review & editing, Validation. **Sonal Khanolkar:** Writing – review & editing, Validation. **Yunpeng Wang:** Writing – review & editing, Validation, Supervision. **Simon C. George:** Writing – review & editing, Writing – original draft, Supervision, Resources, Funding acquisition, Data curation.

Declaration of competing interest

The authors declare that they have no known competing financial interests or personal relationships that could have appeared to influence the work reported in this paper.

Data availability

Data will be made available on request.

Acknowledgements

This research was supported by ANZIC IODP Post Cruise Analytical Funding (PC_SGeorge_0121), the National Natural Science Foundation of China (grant no. 42203029), the Natural Science Foundation of Guangdong Province (grant no. 2024A1515012436), and a Chinese Academy of Sciences President's International Fellowship Initiative grant (no. 2024PVA0106). The authors acknowledge the ship's crew, shipboard IODP staff, and the science party of Expedition 378. We thank the editor and two anonymous reviewers who have helped to improve the quality of this paper.

Appendix A. Supplementary data

Supplementary data to this article can be found online at https://doi.org/10.1016/j.palaeo.2024.112368.

References

Aboglila, S., Grice, K., Trinajstic, K., Snape, C., Williford, K.H., 2011. The significance of 24-norcholestanes, 4-methylsteranes and dinosteranes in oils and source-rocks from East Sirte Basin (Libya). Appl. Geochem. 26, 1694–1705. https://doi.org/10.1016/j.apgeochem.2011.04.026.

Alegret, L., Thomas, E., 2013. Benthic foraminifera across the cretaceous/Paleogene boundary in the Southern Ocean (ODP Site 690): diversity, food and carbonate saturation. Mar. Micropaleontol. 105, 40–51. https://doi.org/10.1016/j.marmicro.2013.10.003.

Barker, C.E., Pawlewicz, M.J., 1994. Calculation of vitrinite reflectance from thermal histories and peak temperatures–a comparison of methods. In: Mukhopadhyay, P.K., Dow, W.G. (Eds.), Vitrinite Reflectance as a Maturity Parameter: Applications and Limitations, vol. 570. American Chemical Society Symposium Series, Washington, DC, p. 294. https://doi.org/10.1021/bk-1994-0570.ch014.

Bein, A., Sofer, Z., 1987. Origin of oils in Helez region, Israel—implications for exploration in the eastern Mediterranean. Am. Assoc. Pet. Geol. Bull. 71, 65–75. https://doi.org/10.1306/94886D49-1704-11D7-8645000102C1865D.

Brune, A., Frenzel, P., Cypionka, H., 2000. Life at the oxic–anoxic interface: microbial activities and adaptations. FEMS Microbiol. Rev. 24, 691–710. https://doi.org/10.1016/S0168-6445(00)00054-1.

Cande, S.C., Stock, J.M., 2004. Pacific-Antarctic-Australia motion and the formation of the Macquarie Plate. Geophys. J. Int. 157, 399–414. https://doi.org/10.1111/j.1365-246X.2004.02224.x.

Carter, R.M., McCave, I.N., Richter, C., Carter, L., et al., 1999. Proceedings of the Ocean Drilling Program, Initial Reports, 181. Texas A&M University, College Station, TX, Ocean Drilling Program. https://doi.org/10.2973/odp.proc.ir.181.2000, 80 pp.

Cathie, B.D., 2020. Cenozoic Evolution of the Campbell Plateau, Subantarctic New Zealand: Insights from Sub-Bottom Profile Data. Master thesis.. School of Geography, Victoria University of Wellington, p. 170 http://researcharchive.vuw.ac.nz/handle/10063/9145.

Clark Jr., R.C, Blumer, M., 1967. Distribution of n-paraffins in marine organisms and sediments. Limnology and Oceanography 12, 79–87. https://doi.org/10.4319/lo.1967.12.1.0079.

Coffin, M.T., Frey, F.A., Wallace, P.J., et al., 2000. Proceedings of the Ocean Drilling Program, Initial Reports, 183. Texas A&M University, College Station, TX, Ocean Drilling Program. https://doi.org/10.2973/odp.proc.ir.183.2000, 101 pp.

Cook, R.A., Sutherland, R., Zhu, H., 1999. Cretaceous-Cenozoic geology and petroleum systems of the Great South Basin, New Zealand. Instit. Geol. Nucl. Sci. 20, 190.

Davey, F.J., Houtz, R.E., 1977. The Campbell Plateau and its relationship with the Ross Sea, Antarctica. Mar. Geol. 25, 61–72. https://doi.org/10.1016/0025-3227(77)90047-0.

Dawson, D., Grice, K., Wang, S.X., Alexander, R., Radke, J., 2004. Stable hydrogen isotopic composition of hydrocarbons in torbanites (Late Carboniferous to Late Permian) deposited under various climatic conditions. Org. Geochem. 35, 189–197. https://doi.org/10.1016/j.orggeochem.2003.09.004.

Didyk, B.M., 1978. Organic geochemical indicators of palaeoenvironmental conditions of sedimentation. Nature 272, 216–222. https://doi.org/10.1038/272216a0.

Eigenbrode, J.L., Freeman, K.H., Summons, R.E., 2008. Methylhopane biomarker hydrocarbons in Hamersley Province sediments provide evidence for Neoarchean aerobiosis. Earth Planet. Sci. Lett. 273, 323–331. https://doi.org/10.1016/j.epsl.2008.06.037.

Exon, N.F., Brinkhuis, H., Robert, C.M., Kennett, J.P., Hill, P.J., Macphail, M.K., 2004. Tectono-sedimentary history of uppermost Cretaceous through Oligocene sequences from the Tasman region, a temperate Antarctic margin. In: Exon, N.F., Kennett, J.P., Malone, M.J. (Eds.), The Cenozoic Southern Ocean: Tectonics, Sedimentation and Climate Change Between Australia and Antarctica, Geophysical Monograph 151. American Geophysical Union, Washington, D.C, pp. 319–344. https://doi.org/10.1029/151GM18.

Farrimond, P., Talbot, H.M., Watson, D.F., Schulz, L.K., Wilhelms, A., 2004. Methylhopanoids: Molecular indicators of ancient bacteria and a petroleum correlation tool. Geochimica et Cosmochimica Acta 68, 3873–3882. https://doi.org/10.1016/j.gca.2004.04.011.

Freeman, K.H., Hayes, J., Trendel, J.-M., Albrecht, P., 1990. Evidence from carbon isotope measurements for diverse origins of sedimentary hydrocarbons. Nature 343, 254–256.

Garcia-Soto, C., Cheng, L., Caesar, L., Schmidtko, S., Jewett, E.B., Cheripka, A., Rigor, I., Caballero, A., Chiba, S., Báez, J.C., Zielinski, T., Abraham, J.P., 2021. An overview of ocean climate change indicators: sea surface temperature, ocean heat content, ocean pH, dissolved oxygen concentration, Arctic Sea ice extent, thickness and volume, sea level and strength of the AMOC (Atlantic Meridional Overturning Circulation). Front. Mar. Sci. 8 https://doi.org/10.3389/fmars.2021.642372, 642372-1-642372-24.

Gersonde, R., Hodell, D.A., Blum, P., et al., 1999. Proceedings of the Ocean Drilling Program, Initial Reports, 177. Texas A & M University, College Station, TX, Ocean Drilling Program. https://doi.org/10.2973/odp.proc.ir.177.1999, 67 pp.

Gillespie, A., Burns, W.C., 2006. Climate Change in the South Pacific: Impacts and Responses in Australia, New Zealand, and Small Island States, vol. 2. Springer Science & Business Media, p. 388. https://doi.org/10.1007/0-306-47981-8.

Goodwin, N.S., Mann, A.L., Patience, R.L., 1988. Structure and significance of C_{30} 4-methyl steranes in lacustrine shales and oils. Org. Geochem. 12, 495–506. https://doi.org/10.1016/0146-6380(88)90159-3.

Gorter, J., 2001. A Marine Source Rock in the Gippsland Basin? Petroleum Exploration Society of Australia, Eastern Australiasian Basins Symposium, Special Publication, Perspective for the Future, Melbourne, pp. 385–390.

Grantham, P.J., Wakefield, L.L., 1988. Variations in the sterane carbon number distributions of marine source rock derived crude oils through geological time. Organic Geochemistry 12, 61–73. https://doi.org/10.1016/0146-6380(88)90115-5.

Grice, K., Audino, M., Boreham, C.J., Alexander, R., Kagi, R.I., 2001. Distributions and stable carbon isotopic compositions of biomarkers in torbanites from different palaeogeographical locations. Org. Geochem. 32, 1195–1210. https://doi.org/10.1016/S0146-6380(01)00087-0.

Grobys, J.W.G., Gohl, K., Uenzelmann-Neben, G., Davy, B., Barker, D., 2009. Extensional and magmatic nature of the Campbell Plateau and Great South Basin from deep crustal studies. Tectonophysics 472, 213–225. https://doi.org/10.1016/j.tecto.2008.05.003.

Hesse, R., Schacht, U., 2011. Chapter 9 - Early diagenesis of deep-sea sediments. In: HüNeke, H., Mulder, T. (Eds.), Developments in Sedimentology, Vol. 63, pp. 557–713. https://doi.org/10.1016/B978-0-444-53000-4.00009-3.

Holba, A.G., Dzou, L.I.P., Masterson, W.D., Hughes, W.B., Huizinga, B.J., Singletary, M. S., Moldowan, J.M., Mello, M.R., Tegelaar, E., 1998a. Application of 24-norcholestanes for constraining source age of petroleum. Org. Geochem. 29, 1269–1283. https://doi.org/10.1016/S0146-6380(98)00184-3.

Holba, A.G., Tegelaar, E.W., Huizinga, B.J., Moldowan, J.M., Singletary, M.S., McCaffrey, M.A., Dzou, L.I.P., 1998b. 24-norcholestanes as age-sensitive molecular fossils. Geology 26, 783–786. https://doi.org/10.1130/0091-7613(1998)026<0783:NAASMF>2.3.CO;2.

Hollis, C.J., Handley, L., Crouch, E.M., Morgans, H.E., Baker, J.A., Creech, J., Collins, K. S., Gibbs, S.J., Huber, M., Schouten, S., Zachos, J.C., Pancost, R.D., 2009. Tropical Sea temperatures in the high-latitude South Pacific during the Eocene. Geology 37, 99–102. https://doi.org/10.1130/G25200A.1.

Hollis, C.J., Tayler, M.J.S., Andrew, B., Taylor, K.W., Lurcock, P., Bijl, P.K., Kulhanek, D. K., Crouch, E.M., Nelson, C.S., Pancost, R.D., Huber, M., Wilson, G.S., Ventura, G.T., Crampton, J.S., Schiøler, P., Phillips, A., 2014. Organic-rich sedimentation in the South Pacific Ocean associated with late Paleocene climatic cooling. Earth Sci. Rev. 134, 81–97. https://doi.org/10.1016/j.earscirev.2014.03.006.

Hollis, C.J., Hines, B.R., Littler, K., Villasante-Marcos, V., Kulhanek, D.K., Strong, C.P., Zachos, J.C., Eggins, S.M., Northcote, L., Phillips, A., 2015. The Paleocene–Eocene Thermal Maximum at DSDP Site 277, Campbell Plateau, southern Pacific Ocean. Clim. Past 11, 1009–1025. https://doi.org/10.5194/cp-11-1009-2015.

Hong, Z.-H., Li, H.-X., Rullkötter, J., Mackenzie, A.S., 1986. Geochemical application of sterane and triterpane biological marker compounds in the Linyi Basin. Org. Geochem. 10, 433–439. https://doi.org/10.1016/0146-6380(86)90043-4.

Hornibrook, N.B., Brazier, R.C., Strong, C.P., 1989. Manual of New Zealand Permian to Pleistocene foraminiferal biostratigraphy. New Zealand Geol. Surv. Paleontol. Bull. 56, 175. https://doi.org/10.2113/gsjfr.21.2.193.

Hoshino, Y., Nettersheim, B.J., Gold, D.A., Hallmann, C., Vinnichenko, G., van Maldegem, L.M., Bishop, C., Brocks, J.J., Gaucher, E.A., 2023. Genetics re-establish the utility of 2-methylhopanes as cyanobacterial biomarkers before 750 million years ago. Nat. Ecol. Evol. 1-10 https://doi.org/10.1038/s41559-023-02223-5.

Huang, W.-Y., Meinschein, W.G., 1979. Sterols as ecological indicators. Geochim. Cosmochim. Acta 43, 739–745. https://doi.org/10.1016/0016-7037(79)90257-6.

Ji, L., Meng, F., Yan, K., Song, Z., 2011. The dinoflagellate cyst Subtilisphaera from the Eocene of the Qaidam Basin, Northwest China, and its implications for hydrocarbon exploration. Rev. Palaeobot. Palynol. 167, 40–50. https://doi.org/10.1016/j.revpalbo.2011.07.005.

Kenig, F., Sinninghe Damsté, J.S., Frewin, N.L., Hayes, J.M., De Leeuw, J.W., 1995. Molecular indicators for palaeoenvironmental change in a Messinian evaporitic sequence (Vena del Gesso, Italy). II: high-resolution variations in abundances and ^{13}C contents of free and Sulphur-bound carbon skeletons in a single marl bed. Org. Geochem. 23, 485–526. https://doi.org/10.1016/0146-6380(95)00049-K.

Kennett, J.P., Houtz, R.E., Andrews, P.B., Edwards, A.R., Gostin, V.A., Hajós, M., Hampton, M., et al., 1975. Cenozoic paleoceanography in the Southwest Pacific Ocean, Antarctic glaciation, and the development of the Circum-Antarctic Current. In: Kennett, J.P., Houtz, R.E., et al. (Eds.), Initial Reports of the Deep Sea Drilling Project, vol. 29. (U.S. Government Printing Office), Washington, D.C., pp. 1155–1169

King, P.R., 2000. New Zealand's changing configuration in the last 100 million years; plate tectonics, basin development, and depositional setting. In: New Zealand Petroleum Conference Proceedings, pp. 131–145. Wellington. https://api.semanticscholar.org/CorpusID:134111013.

Knoll, A.H., Summons, R.E., Waldbauer, J.R., Zumberge, J.E., 2007. Chapter 8: The geological succession of primary producers in the oceans. In: Falkowski, P.G., Knoll, A.H. (Eds.), Evolution of Primary Producers in the Sea. Academic Press, pp. 133–163.

Leinen, M., Rea, D.K., Becker, K., 1986. Deep Sea Drilling Project Leg 92, Southeast Pacific Ocean: Introduction, cruise narrative, principal results, and explanatory notes. In: Leinen, M., Rea, D.K., et al. (Eds.), Initial Reports of the Deep Sea Drilling Project, vol. 92. U.S. Government Printing Office, Washington, D.C., pp. 5–24. https://doi.org/10.2973/dsdp.proc.92.101.1986

Moldowan, J.M., Talyzina, N.M., 1998. Biogeochemical evidence for dinoflagellate ancestors in the early Cambrian. Science 281, 1168–1170. https://doi.org/10.1126/science.281.5380.1168.

Moldowan, J.M., Seifert, W.K., Gallegos, E.J., 1985. Relationship between petroleum composition and depositional environment of petroleum source rocks. AAPG Bull. 69, 1255–1268. https://doi.org/10.1306/AD462BC8-16F7-11D7-8645000102C1865D.

Moldowan, J.M., Fago, F.J., Lee, C.Y., Jacobson, S.R., Watt, D.S., Slougui, N.-E., Jeganathan, A., Young, D.C., 1990. Sedimentary 24-n-propylcholestanes, molecular fossils diagnostic of marine algae. Science 247, 309–312. https://doi.org/10.1126/science.247.4940.309.

Omosanya, K.O., Harishidayat, D., 2019. Seismic geomorphology of Cenozoic slope deposits and deltaic clinoforms in the Great South Basin (GSB) offshore New Zealand. Geo-Mar. Lett. 39, 77–99. https://doi.org/10.1007/s00367-018-00558-8.

Ourisson, G., Rohmer, M., Poralla, K., 1987. Prokaryotic hopanoids and other polyterpenoid sterol surrogates. Annu. Rev. Microbiol. 41, 301–333. https://doi.org/10.1146/annurev.mi.41.100187.001505.

Palliani, R.B., Riding, J.B., 2003. Biostratigraphy, provincialism and evolution of European early Jurassic (Pliensbachian to early Toarcian) dinoflagellate cysts. Palynology 27, 179–214. https://doi.org/10.1080/01916122.2003.9989586.

Peters, K.E., Moldowan, J.M., 1991. Effects of source, thermal maturity, and biodegradation on the distribution and isomerization of homohopanes in petroleum. Org. Geochem. 17, 47–61. https://doi.org/10.1016/0146-6380(91)90039-M.

Peters, K.E., Walters, C.C., Moldowan, J.M., 2005. The Biomarker Guide: Volume 2, Biomarkers and Isotopes in Petroleum Systems and Earth History. Cambridge University Press.

Rampen, S.W., Schouten, S., Abbas, B., Elda Panoto, F., Muyzer, G., Campbell, C.N., Fehling, J., Sinninghe Damsté, J.S., 2007. On the origin of 24-norcholestanes and their use as age-diagnostic biomarkers. Geology 35, 419–422. https://doi.org/10.1130/G23358A.1.

Rashby, S.E., Sessions, A.L., Summons, R.E., Newman, D.K., 2007. Biosynthesis of 2-methylbacteriohopanepolyols by an anoxygenic phototroph. Proc. Natl. Acad. Sci. U. S. A. 104, 15099–15104. https://doi.org/10.1073/pnas.0704912104.

Ricci, J.N., Coleman, M.L., Welander, P.V., Sessions, A.L., Summons, R.E., Spear, J.R., Newman, D.K., 2014. Diverse capacity for 2-methylhopanoid production correlates with a specific ecological niche. ISME J. 8, 675–684. https://doi.org/10.1038/ismej.2013.191.

Rieley, G., Collier, R.J., Jones, D.M., Eglinton, G., 1991. The biogeochemistry of Ellesmere Lake, U.K.-I: source correlation of leaf wax inputs to the sedimentary lipid record. Org. Geochem. 17, 901–912. https://doi.org/10.1016/0146-6380(91)90031-E.

Röhl, U., Thomas, D.J., Childress, L.B., the Expedition 378 Scientists, 2022. South Pacific Paleogene Climate. Proceedings of the International Ocean Discovery Program, 378. International Ocean Discovery Program, College Station, TX. https://doi.org/10.14379/iodp.proc.378.2022.

Rohmer, M., Bouvier-Navé, P., Ourisson, G., 1984. Distribution of hopanoid triterpenes in prokaryotes. Microbiology 130, 1137–1150. https://doi.org/10.1099/00221287-130-5-1137.

Seifert, W.K., Moldowan, J.M., 1980. The effect of thermal stress on source-rock quality as measured by hopane stereochemistry. Phys. Chem. Earth 12, 229–237. https://doi.org/10.1016/0079-1946(79)90107-1.

Seifert, W.K., Moldowan, J.M., 1986. Use of biological markers in petroleum exploration. In: Johns, R.B. (Ed.), Methods in Geochemistry and Geophysics, Vol. 24. Elsevier, Amsterdam, pp. 261–290.

Shanmugam, G., 1985. Significance of coniferous rain forests and related organic matter in generating commercial quantities of oil, Gippsland Basin, Australia. AAPG Bull. 69, 1241–1254. https://doi.org/10.1306/AD462BC3-16F7-11D7-8645000102C1865D.

Sinninghe Damsté, J.S., Kenig, F., Koopmans, M.P., Köster, J., Schouten, S., Hayes, J.M., de Leeuw, J.W., 1995. Evidence for gammacerane as an indicator of water column stratification. Geochim. Cosmochim. Acta 59, 1895–1900. https://doi.org/10.1016/0016-7037(95)00073-9.

Summons, R.E., Jahnke, L.L., Hope, J.M., Logan, G.A., 1999. 2-Methylhopanoids as biomarkers for cyanobacterial oxygenic photosynthesis. Nature 400, 554–557. https://doi.org/10.1038/23005.

Thomas, D.J., Röhl, U., Childress, L.B.A., the Expedition 378 Scientists, 2020. Expedition 378 Preliminary Report: South Pacific Paleogene Climate. International Ocean Discovery Program. https://doi.org/10.14379/iodp.pr.378.2020.

Tissot, B.P., Welte, D.H., 1978. Petroleum Formation and Occurrence: A New Approach to Oil and Gas Exploration. Springer-Verlag, Berlin, New York. https://doi.org/10.1007/978-3-642-87813-8.

Tjalsma, R.C., Lohmann, G.P., 1983. Paleocene-Eocene Bathyal and Abyssal Benthic Foraminifera from the Atlantic Ocean. Micropaleontology Press, American Museum of Natural History, New York, p. 90.

Volkman, J.K., 1986. A review of sterol markers for marine and terrigenous organic matter. Org. Geochem. 9, 83–99. https://doi.org/10.1016/0146-6380(86)90089-6.
Volkman, J.K., 2003. Sterols in microorganisms. Appl. Microbiol. Biotechnol. 60, 495–506. https://doi.org/10.1007/s00253-002-1172-8.
Volkman, J.K., 2005. Sterols and other triterpenoids: source specificity and evolution of biosynthetic pathways. Org. Geochem. 36, 139–159. https://doi.org/10.1016/j.orggeochem.2004.06.013.
Volkman, J.K., Alexander, R., Kagi, R.I., Rowland, S.J., Sheppard, P.N., 1984. Biodegradation of aromatic hydrocarbons in crude oils from the Barrow Sub-basin of Western Australia. Org. Geochem. 6, 619–632. https://doi.org/10.1016/0146-6380(84)90084-6.
Volkman, J.K., Barrett, S.M., Dunstan, G.A., Jeffrey, S., 1993. Geochemical significance of the occurrence of dinosterol and other 4-methyl sterols in a marine diatom. Org. Geochem. 20, 7–15. https://doi.org/10.1016/0146-6380(93)90076-N.
Welander, P.V., Coleman, M.L., Sessions, A.L., Summons, R.E., Newman, D.K., 2010. Identification of a methylase required for 2-methylhopanoid production and implications for the interpretation of sedimentary hopanes. Proc. Natl. Acad. Sci. 107, 8537–8542. https://doi.org/10.1073/pnas.0912949107.
Williams, L.A., 1984. Subtidal stromatolites in Monterey Formation and other organic-rich rocks as suggested source contributors to petroleum formation. AAPG Bull. 68, 1879–1893. https://doi.org/10.1306/AD4619F8-16F7-11D7-8645000102C1865D.
Zundel, M., Rohmer, M., 1985. Hopanoids of the methylotrophic bacteria *Methylococcus capsulatus* and *Methylomonas* sp. as possible precursors of C_{29} and C_{30} hopanoid chemical fossils. FEMS Microbiol. Lett. 28, 61–64. https://doi.org/10.1111/J.1574-6968.1985.TB00764.X.